Research Square

Preprints are preliminary reports that have not undergone peer review.
They should not be considered conclusive, used to inform clinical practice,
or referenced by the media as validated information.

Influence of surface textures and DLC coatings on the tribological behaviour of additively manufactured Ti6Al4V

Lukáš Odehnal

Lukas.Odehnal@vut.cz

Brno University of Technology

Ondřej Kučera

Brno University of Technology

Matúš Ranuša

Brno University of Technology

David Nečas

Brno University of Technology

Ivan Křupka

Brno University of Technology

Martin Hartl

Brno University of Technology

Martin Vrbka

Brno University of Technology

Research Article

Keywords: Additively manufactured Ti6Al4V, Surface texturing, DLC coatings, Protein-rich lubrication.

Posted Date: November 26th, 2026

DOI: https://doi.org/10.21203/rs.3.rs-11775680/v1

License: This work is licensed under a Creative Commons Attribution 4.0 International License.
Read Full License

Additional Declarations: No competing interests reported.

Abstract

Surface texturing and diamond-like carbon (DLC) coatings may improve the tribological performance of additively manufactured Ti6Al4V, but their combined effects under protein-containing lubrication remain unclear. This study compared directly printed and laser-machined dimples and grooves with an untextured reference, each with and without DLC coating. Reciprocating tests against transparent polymethyl methacrylate (PMMA) were conducted in model synovial fluid at 37°C, with three independent specimens per configuration. Simultaneous friction measurements and in situ fluorescence microscopy evaluated friction and the relative fluorescence response of labelled albumin during sliding and static pauses. Most textured surfaces showed recovery or increases in reservoir fluorescence after running-in, with directly printed grooves exhibiting the largest relative increase. DLC-coated specimens showed less visible surface damage but higher mean friction for most configurations. The strongest reservoir fluorescence response did not coincide with the lowest friction. These findings indicate that local fluorescence, visible surface damage and friction reflect distinct aspects of tribological behaviour. Surface optimisation should therefore consider texture geometry and edge morphology alongside coating effects and lubricant redistribution.

1. Introduction

Degenerative and inflammatory joint diseases, including osteoarthritis [1] and rheumatoid arthritis [2], are major causes of pain, impaired mobility, and functional disability and may ultimately require surgical intervention. Despite substantial progress in large joint arthroplasty, the treatment of small joints, particularly the first metatarsophalangeal (1. MTP) joint, remains clinically challenging. Arthrodesis is considered a reliable treatment for advanced 1. MTP joint disease and generally provides favourable functional outcomes [3, 4]. However, because it eliminates joint motion, the choice between arthrodesis and motion-preserving procedures, such as arthroplasty, remains widely discussed, particularly for younger and more active patients [5, 6].

In joint arthroplasty, metal-on-polymer (MoP) bearing couples remain the most widely used configuration. They combine a hard, metallic component with an ultra-high molecular weight polyethylene (UHMWPE) counterface. UHMWPE has become an established articulating polymer owing to its favourable toughness, wear performance, biocompatibility, and long-term clinical record. Nevertheless, wear of the polymeric component remains a critical factor affecting the long-term performance of MoP implants. Sliding against a harder metallic counterface can generate micro- and submicron UHMWPE wear particles [7], which may trigger an adverse biological response, periprosthetic osteolysis, and ultimately aseptic loosening [8, 9] of the implant. Therefore, the selection and surface condition of the metallic counterface are crucial for reducing UHMWPE wear. Cobalt-chromium alloys, such as CoCr30Mo6, have traditionally been favoured for articulating metallic components because of their high hardness and wear resistance. Titanium alloys, particularly Ti6Al4V, are widely used for structural orthopaedic components because of their favourable strength-to-weight ratio, corrosion resistance, biocompatibility, and lower elastic modulus. The lower elastic modulus of Ti6Al4V can help

reduce stress shielding and enhance osseointegration [10, 11]. Ti6Al4V typically has an elastic modulus of approximately 110–114 GPa, whereas CoCr30Mo6 alloys can reach about 210–240 GPa. However, despite these structural advantages, Ti6Al4V exhibits poor tribological performance [12], including a relatively high coefficient of friction (CoF), low resistance to adhesive and abrasive wear, and material degradation associated with repeated disruption of its passive oxide layer [13, 14]. In direct hard-on-soft contact, these limitations may promote abrasive damage to the UHMWPE counterface [15, 16].

Additive manufacturing (AM) technologies, such as Laser Powder Bed Fusion (LPBF), offer a promising route for producing patient-specific Ti6Al4V implants with complex geometries while retaining the biomechanical advantages of titanium [17, 18]. Although AM can provide favourable bulk mechanical properties compared with conventionally processed alloys [19–21], the direct fabrication of articulating bearing surfaces by LPBF remains challenging. The process can leave partially melted powder particles and other surface irregularities attached to the printed surface [22], which may increase abrasive wear of the UHMWPE counterface during articulation. Therefore, post-process finishing is required to obtain a sufficiently smooth bearing surface [23]. However, mechanical polishing can also alter the geometry of intentionally printed surface features or remove them entirely, thereby reducing the potential effectiveness of the AM process [24].

Surface texturing has been widely investigated as a strategy to improve friction and wear behaviour in artificial joint bearing surfaces [25]. Deterministic microtextures can modify local lubrication conditions by altering fluid flow, real contact distribution, and the interaction between the articulating surfaces [26]. Under boundary and mixed lubrication conditions, which are relevant to slow and start-stop joint motion, micro-dimples or grooves may act as lubricant reservoirs, supporting local replenishment of lubricant within the contact [27, 28]. Compared with directly printed surface structures, laser micromachining offers a flexible post-processing route for producing well-defined textures on already finished Ti6Al4V surfaces [29–31]. This approach can improve geometric control of texture shape, size, and spatial distribution while avoiding subsequent removal or deformation of texture features during mechanical polishing. However, surface texturing alone does not overcome the limited hardness and wear resistance of titanium alloys. Therefore, texturing can be combined with DLC coatings, which may improve the protection of the titanium substrate and reduce direct metallic wear under boundary-lubricated sliding conditions [32]. At the same time, combining hard coatings with surface textures may introduce additional risks in hard-on-soft contacts. If laser-machined textures contain sharp edges, steep sidewalls, or material pile-ups, the subsequent hard coating may preserve these topographical discontinuities and increase local stress concentrations at the UHMWPE counterface. Since texture edge geometry has been shown to influence interlocking and tribological behaviour in MoP bioimplant contacts [33], the interaction between laser-textured DLC-coated Ti6Al4V surfaces and softer UHMWPE counterfaces requires further investigation.

The performance of these surface topographies is strongly influenced by their interaction with synovial fluid (SF) [34]. In boundary lubrication, proteins contained in SF can adsorb onto articulating surfaces and contribute to the formation of a protective interfacial layer. This behaviour is related to the

mechanism described by Myant et al. [35, 36] as Protein Aggregation Lubrication (PAL), in which proteins accumulate and reorganise within the contact under sliding conditions. Such protein-rich layers can influence friction by modifying the local shear response of the lubricant film. *In situ* fluorescence microscopy offers a useful approach to observe these processes directly within the contact region [37, 38].

Our previous study [39] investigated the long-term wear behaviour and durability of additively manufactured Ti6Al4V surfaces, highlighting the relevance of controlled surface structures for joint implant applications. The unresolved design question is whether combining surface textures with DLC coatings improves lubricant availability and surface protection while also reducing friction. Local lubricant accumulation need not produce a low-shear interface, and a protective coating may change friction independently of visible surface damage. We therefore combine in situ fluorescence imaging, simultaneous friction measurements and surface characterisation to examine these responses across laser-machined and additively manufactured textures, with and without DLC. The comparison concerns the resulting surface configurations rather than an isolated manufacturing-process effect. The study addresses two questions:

- **Texture geometry and lubrication**: how the tested surface configurations influence local lubricant distribution during sliding and static pauses, using labelled albumin as an optical tracer within a multicomponent model synovial fluid.
- **Coating and tribological response**: whether DLC-associated changes in surface damage and friction correspond to changes in the local fluorescence response.

2. Materials and methods

Experimental apparatus

Experiments were conducted on a custom-made reciprocating pin-on-plate tribometer (Fig. 1). The metallic pin remained stationary in a lubricant bath maintained at 37°C, while the transparent PMMA plate reciprocated. A feedback loop controlled the normal load, and a strain gauge sensor recorded the friction force at 50 Hz. In situ images were acquired using a fluorescence microscope (Nikon Eclipse Ni, Japan) with a 5× objective, filters matched to rhodamine-B-isothiocyanate (RBITC), and an sCMOS camera (ANDOR Neo 5.5, UK).

Test specimens and lubricant

The study evaluated 3D printed Ti6Al4V pins with a nominal radius of 100 mm. Two distinct categories of surface modifications were investigated: structures produced directly during 3D printing and structures created post-printing via laser surface texturing. In addition, both uncoated and DLC-coated samples were included in the study. As a counterpart, transparent polymethyl methacrylate (PMMA) plates were used for *in situ* optical fluorescence observation, since one component had to be transparent.

All tested pins were fabricated from Ti6Al4V ELI powder (Carpenter Additive) using the Laser Powder Bed Fusion process on an SLM 280^{HL} 3D printer (Nikon SLM Solutions AG, Lübeck, Germany). The system was equipped with a 700 W YLR-700-WC-Y11 fibre laser with an 82 µm focal diameter and a Gaussian power distribution. Argon was used as the protective gas, maintaining the oxygen content below 0.05%. The powder bed was preheated to 200°C. For the AM structures category, topographies were generated directly during printing using two distinct meander printing strategies: the first with 90° rotation between layers (creating regularly spaced AM dimples) and the second with 0° rotation between layers (creating regularly arranged AM grooves). Both printing strategies were applied exclusively to the upper 2 mm of the pin, while the remaining volume was produced as a homogeneous material. The processing parameters were set as follows: layer thickness of 30 µm, hatch distance of 179 µm, laser power of 100 W, and scan speed of 450 mm/s. Laser dimples and Laser grooves were fabricated using an Nd:YAG laser only after the initial smooth spherical cap had been fully polished. The laser operated at a wavelength of 1030 nm, a pulse length of 1 ps, a repetition rate of 60 kHz, and a maximum pulse energy of 1 mJ. The nominal laser-texture geometry comprised a square array of circular dimples, 50 µm in diameter and 120 µm deep, with a centre-to-centre spacing of 180 µm in both directions, and parallel grooves, 35 µm wide and 120 µm deep, with a centre-to-centre spacing of 180 µm. To evaluate the effect of a hard protective coating, a DLC layer with a total thickness of 2.5 µm was applied to half of the prepared surfaces. The coating consisted of a Cr + WC:H + DLC multilayer system and was deposited using a combination of magnetron sputtering and plasma-enhanced chemical vapour deposition (PECVD). The coating was applied after final surface preparation, including polishing and, where applicable, laser texturing. Adhesion was classified as HF2 according to VDI 3198.

Therefore, the experimental matrix (see Table 1) included five surface topographies prepared on additively manufactured Ti6Al4V pins: a smooth untextured reference, laser-machined dimples, laser-machined grooves, directly printed AM dimples, and directly printed AM grooves. Each topography was evaluated under two surface conditions: uncoated and DLC-coated.

Table 1
Experimental matrix of the investigated surface conditions.

	Untextured		**Dimples**		**Grooves**	
	Uncoated	**DLC**	**Uncoated**	**DLC**	**Uncoated**	**DLC**
Polished reference	3	3	–	–	–	–
Laser micromachining	–	–	3	3	3	3
Direct LPBF texturing	–	–	3	3	3	3
Values indicate the number of independent specimens per configuration.						

Prior to tribological testing, all titanium pins were polished according to the standards of the joint replacement manufacturer. Subsequently, the surface topography of all pins was evaluated using a 3D optical profilometer (Bruker Contour GTX). The initial surface roughness (S_a), measured on the

expected contact area after polishing of the samples, was approximately 60 ± 5 nm for all specimens, ensuring a comparable starting finish. The actual radius of curvature extracted from the 3D scans yielded mean values close to the nominal 100 mm (typical measured values: 98.5–101.2 mm). Based on these measured radii and the material properties of Ti6Al4V (Young's modulus: 114 GPa, Poisson's ratio: 0.34) and PMMA (Young's modulus: 3.35 GPa, Poisson's ratio: 0.36), the theoretical Hertzian contact parameters under a 5 N load were calculated, resulting in a theoretical contact radius (a) of ≈ 465 µm and an estimated maximum contact pressure (p_{max}) of ≈ 11 MPa.

The lubricant employed in the experiments was a synthetically prepared model synovial fluid (M-SF) that mimics the composition of human synovial fluid obtained from patients following total joint arthroplasty [34]. The solution was based on phosphate-buffered saline (PBS), in which key SF constituents were diluted: albumin (26.3 mg/ml), γ-globulin (8.2 mg/ml), hyaluronic acid (0.82 mg/ml), and phospholipids (0.35 mg/ml). For *in situ* fluorescence microscopy, albumin was labelled with RBITC because it was the most abundant protein in the model fluid. It served as an optical tracer for examining local lubrication behaviour in the multicomponent fluid. This selective labelling does not resolve the individual contributions of the other constituents or their interactions.

Experimental procedures and data evaluation

Before the experiments, we developed customised automated computational routines in Python to accurately quantify micro-texture geometries using an "adaptive ring method", an algorithm that radially evaluates local pile-up elevation and reservoir depth relative to the adjacent unworn surface by progressively expanding concentric zones outward from each texture's centroid (see results in Fig. 2).

The kinematic and loading conditions were set as follows: a load of 5 N, a stroke length of 20 mm, and a sliding velocity of 20 mm/s, resulting in a frequency of 0.5 Hz. A total of 100 sliding cycles were performed. The experiments were designed to examine local lubricant redistribution during alternating sliding intervals and static pauses. The experimental sequence consisted of four separate dynamic measurements, each lasting 25 sliding cycles and including a 5-minute static pause under a 5 N load. Consequently, the results were divided into an initial run-in phase (the first 25 cycles, designated − 25 to 0) and a subsequent post-run-in phase consisting of the remaining three dynamic measurements (cycles 0 to 75). The obtained fluorescence images were processed using custom-written MATLAB scripts. The normalised fluorescence intensity ($I/I_0 - 1$) was calculated for both the entire contact area and the specific texture reservoirs to characterise relative temporal changes in the fluorescence signal of labelled albumin. To accurately reflect the fluid dynamics, the acquired intensity (I) was normalised against a baseline reference image (I_0) captured at the exact beginning of the post-run-in phase (cycle 0), immediately following the first 5-minute static pause.

3. Results

Initial surface topography and texture geometry

The tested textures differed in both area coverage and characteristic dimensions (Fig. 2). Laser-machined dimples had an area coverage of 5.82 ± 0.32%, compared with 1.55 ± 0.33% for AM dimples. AM grooves exhibited substantial variability in area coverage (19.24 ± 9.42%) and width (45.00 ± 41.05 µm). The DLC-coated laser grooves showed a markedly higher near-edge elevation than the other configurations.

Frictional Behaviour

The coefficient of friction was recorded continuously during the *in situ* fluorescence experiments. Figure 3 compares the CoF of the reference and textured surfaces with and without a DLC coating at the stabilised post-run-in phase. For the uncoated samples, the mean CoF ranged from approximately 0.29 to 0.33. The lowest mean value was observed for the laser-grooved surface, whereas the laser-dimpled surface exhibited the highest CoF among the textured samples. The DLC coating effect depended on surface topography. For the reference sample, the DLC coating increased the CoF from approximately 0.31 to 0.41. An increase was also observed for the laser-grooved, AM-dimpled, and AM-grooved surfaces, reaching values of approximately 0.33, 0.36, and 0.37, respectively. In contrast, the DLC-coated laser-dimpled surface showed a slight decrease in CoF compared with its uncoated counterpart. The laser-grooved samples showed the greatest variability, as indicated by the relatively wide error bars.

The detailed time evolution of CoF for all tested specimens is shown in Fig. 4. In both surface conditions, the largest variations were observed during the initial run-in phase. After this phase, the friction curves became more stable, although local fluctuations were still observed after the static pauses.

Surface integrity

After short-term *in situ* tribological tests against PMMA counterfaces, the surface condition of the Ti6Al4V pins was evaluated by comparing pre- and post-test 3D topography scans and by optical inspection of the tested contact areas. The change in areal roughness, expressed as ΔS_a remained low across all tested groups, in the tens of nanometres.

From the images of the contact area after experiments, the semi-quantitative optical wear severity index was evaluated. It is based on the degree of wear on the contact surface and is divided into 5 categories, characterised by the extent or depth of the dominant grooves following a friction test (ranging from 1 – no wear to 5 – maximum wear). It showed generally higher values for the uncoated Ti6Al4V specimens than for the corresponding DLC-coated specimens (see Fig. 5).

The uncoated reference, laser dimpled, AM dimpled and laser grooved surfaces exhibited visible scratches oriented mainly along the sliding direction. The highest mean severity index was observed in the uncoated groups for the laser-grooved surface. In contrast, the AM-grooved surface showed less optical damage than the other uncoated textured variants. In the DLC-coated groups, the severity index was lower for all corresponding topographies. The representative optical images in Fig. 6 show fewer visible scratches on the DLC-coated specimens compared with the uncoated specimens. The texture

reservoirs remained visible after testing for both laser-machined and directly printed textures, with no obvious loss of texture geometry in the tested contact regions.

Lubricant film dynamics (in situ fluorescence)

The distribution of the fluorescently labelled albumin in the contact was evaluated from the *in situ* fluorescence images. Brighter regions indicate a higher detected fluorescence signal from labelled albumin; the signal was not calibrated to absolute albumin concentration or lubricant-film thickness. Representative image sequences for all tested groups are shown in Fig. 7. The images illustrate the evolution of fluorescence intensity during the run-in phase and during the subsequent sliding intervals separated by static pauses.

For the quantitative evaluation, fluorescence intensity was analysed separately within the texture reservoirs and on the contact plateau outside the textures. For the untextured reference surfaces, the intensity was evaluated over the corresponding contact area. The time evolution of the normalised fluorescence intensity is shown in Fig. 8. The untextured reference surfaces showed a decrease in normalised fluorescence intensity during the test. The uncoated reference intensity decreased below the baseline during the post-run-in phase. A similar decreasing trend was also observed for the DLC-coated reference. In contrast, most textured surfaces showed an increase or partial recovery of fluorescence intensity inside the texture regions after the initial run-in phase.

For the uncoated textured surfaces, the most pronounced increase in fluorescence intensity inside the texture reservoirs was observed for the AM grooves and AM dimples. The uncoated laser grooves and laser dimples showed smaller increases, with normalised reservoir fluorescence remaining above that of the untextured reference during the post-run-in phase. For the DLC-coated textured surfaces, AM grooves showed the highest increase in reservoir intensity. The laser dimples and laser grooves also showed positive normalised intensity values during the post-run-in phase. In contrast, the AM dimples remained close to the baseline or slightly below it.

Outside the textures, the uncoated surfaces showed larger differences between individual topographies than the DLC-coated surfaces. The uncoated AM dimples exhibited the highest normalised fluorescence intensity on the contact plateau, followed by the uncoated laser grooves and AM grooves. The uncoated laser dimples and uncoated reference remained close to or below the baseline. In the DLC-coated groups, normalised intensity outside the textures remained mostly near baseline or slightly negative for most topographies. A transient increase was observed for the DLC-coated laser dimples during the early part of the post-run-in phase. Fluorescence intensity was generally higher immediately after static holds than before them and subsequently decreased during resumed sliding. The magnitude of these changes varied among the tested surface configurations.

Figure 9 shows the spatial distribution of fluorescence within and around the texture features. For laser-machined dimples, high-intensity regions frequently occurred near the dimple edges and along the adjacent surface. For directly printed AM dimples, the high-intensity regions were distributed more

irregularly within the printed texture features. Elongated fluorescent regions were also observed next to selected texture features, with their orientation related to the sliding direction. These spatial patterns differed between laser-machined and directly printed textures.

4. Discussion

This study combined in situ fluorescence imaging, simultaneous friction measurements and surface characterisation to examine the effects of surface texture and DLC coating on additively manufactured Ti6Al4V under protein-containing lubrication. The central finding is that local reservoir fluorescence, visible surface damage and friction did not vary together: DLC reduced visible damage but generally increased friction, while the largest reservoir fluorescence response did not correspond to the lowest friction.

Texture geometry and lubricant redistribution

The differences between the laser-machined and directly 3D printed surfaces should be interpreted in the context of their distinct geometric characteristics. The investigated textures were not geometrically identical features produced by two alternative manufacturing techniques. Instead, the manufacturing routes resulted in different area coverages, characteristic dimensions, spatial regularities, and edge morphologies (see Fig. 2). Consequently, the manufacturing route cannot be fully separated from the resulting texture geometry.

Previous studies have demonstrated that the tribological performance of surface textures depends not only on their presence but also on their dimensions, area coverage, aspect ratio, arrangement, and orientation relative to the sliding direction [27, 28]. Pettersson et al. [32] showed that the ability of textured DLC surfaces to supply lubricant into a boundary-lubricated contact and isolate wear debris was strongly related to the shape, dimensions, and orientation of the texture pattern. Similarly, our previous investigation [33] of textured Ti6Al4V surfaces demonstrated that texture depth and rim morphology can substantially affect lubricant-film formation and friction.

Laser machining produced comparatively regular texture features but also generated local pile-ups and pronounced edge transitions. These elevated rims may alter the local contact-pressure distribution and mechanically interact with the counterface. Previous work [33] on laser-textured Ti6Al4V shows that sharp texture rims can scratch a softer counter-surface and increase friction. In contrast, the directly printed textures exhibited greater dimensional and spatial variability, which may have affected local fluid accommodation. Therefore, the observed differences should be attributed to the combined effects of the manufacturing route and the resulting topography rather than to the manufacturing process alone.

The untextured reference surfaces exhibited a progressive decrease in normalised fluorescence intensity. In contrast, most textured surfaces showed either recovery or an increase in the signal within the texture regions after the run-in phase. This behaviour is consistent with texture features locally accumulating fluorescently labelled albumin. The increases in fluorescence intensity observed during the

static pauses, followed by decreases after reciprocating motion was resumed, are consistent with local accumulation and redistribution, although fluid exchange cannot be distinguished from adsorption or aggregation using fluorescence alone.

The transient character of this behaviour agrees with previous observations of protein-rich lubrication in artificial joint contacts. Myant et al. [35] showed that protein aggregate formation and the stability of protein-rich films are sensitive to transient entrainment conditions. Direct optical observations in knee and hip replacement models further show that SF constituents can accumulate, reorganise, and form boundary layers during articulation [37]. Accordingly, the fluorescence signal recorded in the present study should be interpreted as a relative measure of the spatial distribution of labelled albumin rather than as a direct measurement of total lubricant-film thickness or absolute protein concentration. The signal may have been affected by the local volume of fluorescent fluid within the optical path, adsorption of labelled albumin, texture depth, and differences in the optical response of coated and uncoated surfaces.

Among the textured surfaces, the AM grooves exhibited the largest increase in fluorescence signal within the texture reservoirs in both surface conditions. This response may be associated with their relatively high area coverage, elongated geometry, and orientation relative to the sliding direction. Because each fluorescence response was normalised to its own baseline, a larger relative increase does not establish greater absolute albumin retention than in another group. Grooves can provide extended pathways for fluid transport, whereas isolated dimples depend more strongly on local exchange with the surrounding contact plateau [27, 28, 32]. Nevertheless, the high geometrical variability of the AM grooves indicates that filling and release were unlikely to be spatially uniform across the contact.

The spatial fluorescence patterns also differed between the two dimpled surfaces. The laser-machined dimples showed comparatively localised high-intensity regions near their edges, whereas the signal associated with the directly printed AM dimples was distributed more irregularly. The elongated fluorescent regions extending from selected features in the sliding direction may indicate redistribution of labelled albumin from the texture reservoirs to the adjacent contact plateau. These observations are consistent with redistribution from the textures, but do not directly establish the rate or direction of lubricant transport.

Surface protection and frictional response

The lower optical wear severity observed for the DLC-coated specimens is consistent with reduced visible surface damage during sliding against PMMA. The texture reservoirs remained visible after testing, and no obvious loss of texture geometry was detected. This protective response is consistent with the high hardness and wear resistance generally associated with DLC-based coatings. In contrast, DLC deposition did not generally reduce friction. The largest increase was observed for the untextured reference, for which the mean CoF increased from approximately 0.31 to 0.41. Increased CoF was also observed for the laser-grooved and both directly printed surfaces. The laser-dimpled surface was the only configuration that showed a slight reduction in CoF after DLC deposition. The simultaneous

reduction in visible surface damage and increase in friction is not contradictory. Since the largest CoF increase occurred on the untextured reference, texture-edge interactions alone cannot explain the overall coating-associated friction response. Surface protection and interfacial friction describe different aspects of the tribological response. The DLC layer may resist scratching and direct damage to the titanium substrate. At the same time, the friction force may be influenced by shearing of the interfacial protein-rich layer, the real load-bearing area, coating chemistry, and local surface geometry.

The literature also shows that DLC does not have a universal frictional response in biological lubricants. Anil et al. [40] found that the tribological behaviour of DLC and Si-DLC coatings on Ti6Al4V was strongly influenced by the surrounding medium and surface modification, with bovine serum producing a different response from water or ambient air. Xu and Pruitt [41] reported improved friction and wear performance for DLC-coated Ti6Al4V against medical-grade UHMWPE, but also demonstrated that the response depended on coating structure, surface roughness, and lubrication. Ghosh et al. [42] reported lower friction and wear for a DLC-coated micro-dimpled surface in an osteoarthritis-oriented synovial fluid than for plain and uncoated dimpled surfaces. This differs from the general increase in CoF observed after DLC deposition in the present study. Recent experiments on DLC-coated biomedical alloys also showed that friction depended on coating composition and material combination [43]. This apparent discrepancy emphasises that the performance of a textured DLC surface depends on the complete tribological system, including texture dimensions, coating composition, counterface material, contact pressure, sliding kinematics, and lubricant formulation [32, 42]. Guo et al. [44] reported higher friction under BSA lubrication than in water or NaCl solution for a DLC-coated CoCrMo contact, illustrating that protein-containing lubrication does not necessarily minimise friction on DLC surfaces.

The results did not reveal a simple relationship between the fluorescence signal within the textures and macroscopic CoF. For example, the DLC-coated AM grooves exhibited the strongest increase in reservoir fluorescence but also one of the highest CoF values among the coated textured surfaces. Conversely, the laser-machined dimples did not show the strongest reservoir signal but were the only texture where DLC deposition slightly reduced CoF.

These observations suggest that the relative reservoir fluorescence signal alone is insufficient to explain the frictional performance of the tested surfaces. A high fluorescence signal within a reservoir does not necessarily imply the formation of a continuous low-shear film across the load-bearing plateau. The retained fluid must also be transported from the reservoir to the regions supporting the normal load. Moreover, the frictional response of protein-containing lubricants can increase as protein-rich layers accumulate and are subsequently sheared within the contact [33, 35–38]. Previous experiments on textured Ti6Al4V similarly showed that increased protein-film formation was not necessarily accompanied by reduced CoF [33]. Experiments on DLC films have shown that albumin and γ-globulin can produce different adsorption and wear responses, indicating that the signal from labelled albumin alone does not describe the contribution of all proteins to interfacial lubrication [45].

The macroscopic friction response was therefore probably determined by several concurrent mechanisms: local fluid retention and release, adsorption and shear of the protein-rich boundary layer, the fraction and distribution of the load-bearing plateau, and mechanical interactions at the texture edges. Consequently, a texture's effectiveness should be evaluated not only by its apparent storage capacity but also by its ability to redistribute lubricant without introducing mechanically unfavourable surface discontinuities.

Limitations and implications for surface design

Several limitations should be considered when interpreting the findings. The primary experiments were short-term tests against an optically transparent PMMA counterface and therefore did not reproduce the mechanical and surface properties of a clinical UHMWPE bearing. Only fluorescently labelled albumin was observed, although the model synovial fluid also contained globulin, hyaluronic acid, and phospholipids. The measured fluorescence intensity represented a relative optical signal rather than a calibrated measurement of film thickness or local protein concentration. In addition, the geometries of the laser-machined and directly printed textures were not matched, preventing complete separation of manufacturing-route and geometry effects. The three independent specimens per primary group limit the precision of comparisons, particularly where variability is substantial.

Within the tested conditions, DLC deposition did not consistently reduce friction. Future optimisation should consider texture area coverage, depth, edge morphology, orientation and coating conformity together with lubricant redistribution. Replicated long-term experiments against UHMWPE are required to determine whether the tested surface configurations improve polymer wear performance; the present PMMA experiments do not establish this outcome.

5. Conclusions

This study investigated the short-term effects of directly printed and laser-machined textures combined with DLC coatings on the tribological behaviour of additively manufactured Ti6Al4V, while four principal findings were obtained:

- Surface textures modified the spatial distribution and temporal evolution of the fluorescently labelled albumin signal, particularly during the post-run-in phase and after static pauses.
- The response depended on the resulting texture topography, with directly printed AM grooves showing the most pronounced increase in fluorescence signal within the texture regions.
- The DLC coating reduced the optically observed surface damage of the Ti6Al4V specimens but did not systematically reduce friction. Instead, the coating increased the mean coefficient of friction for most surface configurations, with laser-machined dimples representing the only exception.
- The combined experimental approach allowed local fluorescence changes to be examined alongside friction and visible surface damage across additively manufactured and laser-machined

textures. It revealed that a strong reservoir fluorescence response alone does not identify a low-friction surface configuration.

These findings suggest that the labelled-albumin fluorescence response, optically observed surface damage, and macroscopic friction reflect related but distinct aspects of the tribological response. Overall, the results show that optimising DLC-coated textured surfaces must consider not only lubricant-retention capacity, but also texture geometry, edge morphology, coating conformity, and mechanical interaction with the polymer counterface.

Declarations

Declaration of generative AI and AI-assisted technologies in the writing process

During the preparation of this work, the authors used ChatGPT and Grammarly to improve language quality and readability. After using these tools, the authors reviewed and edited the content as needed and take full responsibility for the publication's content.

Declaration of Competing Interest

The authors declare that they have no known competing financial interests or personal relationships that could have appeared to influence the work reported in this paper.

Author Contribution

L. Odehnal, M. Ranuša, and M. Vrbka conceived the idea. L. Odehnal, O. Kučera, and M. Ranuša designed the experiments. O. Kučera performed the experiments and analysed the data. L. Odehnal wrote the original draft of the manuscript. M. Ranuša, D. Nečas, M. Vrbka revised the manuscript. M. Vrbka, M. Hartl, and D. Nečas administrated the projects and secured the funding. I. Křupka supervised the study.

Acknowledgment

This research was supported by the project *"3D printed individualised segmental joint implant: optimisation of fixation to bone and biotribology of articular surface"*, funded as project No. NW25-08-00044 by the Ministry of Health of the Czech Republic in cooperation with the Czech Health Research Council, by the project *"Mechanical Engineering of Biological and Bio-inspired Systems"*, funded as project No. CZ.02.01.01/00/22_008/0004634 by Programme Johannes Amos Comenius, call Excellent Research, administered by the Ministry of Education, Sports and Youth and by the project *"3D printed metal matrix composites"*, funded as project No. 25-15390S by the Czech Science Foundation.

Data Availability

The data supporting the findings of this study are openly available in the Zenodo repository at https://doi.org/10.5281/zenodo.23945599.

References

1. Tang, S., Zhang, C., Oo, W.M., Fu, K., Risberg, M.A., Bierma-Zeinstra, S.M., et al.: Osteoarthr. Nat. Rev. Dis. Primers. **11**, 10 (2025). https://doi.org/10.1038/s41572-025-00594-6
2. Smolen, J.S., Aletaha, D., Barton, A., Burmester, G.R., Emery, P., Firestein, G.S., et al.: Rheumatoid arthritis. Nat. Rev. Dis. Primers. **4**, 18001 (2018). https://doi.org/10.1038/nrdp.2018.1
3. Brewster, M.: Does Total Joint Replacement or Arthrodesis of the First Metatarsophalangeal Joint Yield Better Functional Results? A Systematic Review of the Literature. J. Foot Ankle Surg. **49**, 546–552 (2010). https://doi.org/10.1053/j.jfas.2010.07.003
4. Jadhakhan, F., Nilesh, M., Lyndon, M., Paul, H., Alison, R.: Clinical Outcomes of First Metatarsophalangeal Joint Arthrodesis Using the BOFAS Registry: A Prospective Cohort Study. J. Foot Ankle Res. 18 (2025). https://doi.org/10.1002/jfa2.70084
5. França, G., Nunes, J., Pinho, P., Freitas, D., Andrade, R., Espregueira-Mendes, J., et al.: Is arthrodesis still the best treatment option for first metatarsophalangeal joint arthritis?—a systematic review of arthrodesis and arthroplasty outcomes. Ann. Jt. **6**, 5–5 (2021). https://doi.org/10.21037/aoj-20-88
6. Polzer, H.: Hallux rigidus: Joint preserving alternatives to arthrodesis - a review of the literature. World J. Orthop. **5**, 6 (2014). https://doi.org/10.5312/wjo.v5.i1.6
7. Stratton-Powell, A.A., Tipper, J.L., Biomaterials Handbook, U.H.M.W.P.E.: Elsevier; pp. 635–653. (2016). https://doi.org/10.1016/B978-0-323-35401-1.00033-8
8. Atkins, G.J.: Role of polyethylene particles in peri-prosthetic osteolysis: A review. World J. Orthop. **2**, 93 (2011). https://doi.org/10.5312/wjo.v2.i10.93
9. Kandahari, A.M., Yang, X., Laroche, K.A., Dighe, A.S., Pan, D., Cui, Q.: A review of UHMWPE wear-induced osteolysis: the role for early detection of the immune response. Bone Res. **4**, 16014 (2016). https://doi.org/10.1038/boneres.2016.14
10. Marin, E., Lanzutti, A.: Biomedical Applications of Titanium Alloys: A Comprehensive Review. Materials. **17**, 114 (2023). https://doi.org/10.3390/ma17010114
11. Bandyopadhyay, A., Mitra, I., Goodman, S.B., Kumar, M., Bose, S.: Improving biocompatibility for next generation of metallic implants. Prog Mater. Sci. **133**, 101053 (2023). https://doi.org/10.1016/j.pmatsci.2022.101053
12. Long, M., Rack, H.J.: Titanium alloys in total joint replacement—a materials science perspective. Biomaterials. **19**, 1621–1639 (1998). https://doi.org/10.1016/S0142-9612(97)00146-4
13. Doni, Z., Alves, A.C., Toptan, F., Gomes, J.R., Ramalho, A., Buciumeanu, M., et al.: Dry sliding and tribocorrosion behaviour of hot pressed CoCrMo biomedical alloy as compared with the cast

CoCrMo and Ti6Al4V alloys. Mater. Des. (1980–2015). **52**, 47–57 (2013). https://doi.org/10.1016/j.matdes.2013.05.032

14. Abd-Elaziem, W., Darwish, M.A., Hamada, A., Daoush, W.M.: Titanium-Based alloys and composites for orthopedic implants Applications: A comprehensive review. Mater. Des. **241**, 112850 (2024). https://doi.org/10.1016/j.matdes.2024.112850
15. Guezmil, M., Bensalah, W., Mezlini, S.: Tribological behavior of UHMWPE against TiAl6V4 and CoCr28Mo alloys under dry and lubricated conditions. J. Mech. Behav. Biomed. Mater. **63**, 375–385 (2016). https://doi.org/10.1016/j.jmbbm.2016.07.002
16. Feldshtein, E.E., Vitjaz, P.A., Leksycki, K.: Tribotechnical Characteristics of Ti6Al4V Titanium Alloy–Ultra-High-Molecular-Weight Polyethylene Friction Pairs. J. Frict. Wear. **41**, 399–404 (2020). https://doi.org/10.3103/S1068366620050098
17. Das, A., Rajkumar, P.: Metal 3D printing of biometals for prostheses and implants: a review. Exploration of BioMat-X 2025;2. https://doi.org/10.37349/ebmx.2025.101338
18. Mohammed, M.T., V G S, A V S: SLM-built titanium materials: great potential of developing microstructure and properties for biomedical applications: a review. Mater. Res. Express. **6**, 122006 (2020). https://doi.org/10.1088/2053-1591/ab624c
19. Bartolomeu, F., Gasik, M., Silva, F.S., Miranda, G.: Mechanical Properties of Ti6Al4V Fabricated by Laser Powder Bed Fusion: A Review Focused on the Processing and Microstructural Parameters Influence on the Final Properties. Met. (Basel). **12**, 986 (2022). https://doi.org/10.3390/met12060986
20. Rafi, H.K., Karthik, N.V., Gong, H., Starr, T.L., Stucker, B.E.: Microstructures and Mechanical Properties of Ti6Al4V Parts Fabricated by Selective Laser Melting and Electron Beam Melting. J. Mater. Eng. Perform. **22**, 3872–3883 (2013). https://doi.org/10.1007/s11665-013-0658-0
21. Jeyaprakash, N., Yang, C.-H., Prabu, G., Radhika, N.: Mechanism Correlating Microstructure and Wear Behaviour of Ti-6Al-4V Plate Produced Using Selective Laser Melting. Met. (Basel). **13**, 575 (2023). https://doi.org/10.3390/met13030575
22. Zhang, Y., Li, J., Che, S., Tian, Y.: Electrochemical Polishing of Additively Manufactured Ti–6Al–4V Alloy. Met. Mater. Int. **26**, 783–792 (2020). https://doi.org/10.1007/s12540-019-00556-0
23. Hashmi, A.W., Mali, H.S., Meena, A., Saxena, K.K., Ahmad, S., Agrawal, M.K., et al.: A comprehensive review on surface post-treatments for freeform surfaces of bio-implants. J. Mater. Res. Technol. **23**, 4866–4908 (2023). https://doi.org/10.1016/j.jmrt.2023.02.007
24. Ranuša, M., Čípek, P., Vrbka, M., Paloušek, D., Křupka, I., Hartl, M.: Tribological behaviour of 3D printed materials for small joint implants: A pilot study. J. Mech. Behav. Biomed. Mater. **132**, 105274 (2022). https://doi.org/10.1016/j.jmbbm.2022.105274
25. Allen, Q., Raeymaekers, B.: Surface Texturing of Prosthetic Hip Implant Bearing Surfaces: A Review. J. Tribol. 143 (2021). https://doi.org/10.1115/1.4048409
26. Grützmacher, P.G., Profito, F.J., Rosenkranz, A.: Multi-Scale Surface Texturing in Tribology—Current Knowledge and Future Perspectives. Lubricants. **7**, 95 (2019).

https://doi.org/10.3390/lubricants7110095

27. Shen, G., Zhang, J., Culliton, D., Melentiev, R., Fang, F.: Tribological study on the surface modification of metal-on-polymer bioimplants. Front. Mech. Eng. **17**, 26 (2022). https://doi.org/10.1007/s11465-022-0682-6
28. Shen, G., Zhang, J., Kang, C., Fang, F.: Study on surface texture patterns for improving tribological performance of bioimplants. Surf. Coat. Technol. **422**, 127567 (2021). https://doi.org/10.1016/j.surfcoat.2021.127567
29. Prasad, K.N., Syed, I., Subbu, S.K.: Laser dimple texturing – applications, process, challenges, and recent developments: a review. Australian J. Mech. Eng. **20**, 316–331 (2022). https://doi.org/10.1080/14484846.2019.1705533
30. Woźniak, A., Bialas, O., Adamiak, M., Hadzima, B., Szewczenko, J.: The influence of laser texturing on the tribological behavior of titanium alloy Ti6Al4V in medical applications. Archives Civil Mech. Eng. **24**, 146 (2024). https://doi.org/10.1007/s43452-024-00960-3
31. Lin, N., Li, D., Zou, J., Xie, R., Wang, Z., Tang, B.: Surface Texture-Based Surface Treatments on Ti6Al4V Titanium Alloys for Tribological and Biological Applications: A Mini Review. Materials. **11**, 487 (2018). https://doi.org/10.3390/ma11040487
32. Pettersson, U., Jacobson, S.: Friction and Wear Properties of Micro Textured DLC Coated Surfaces in Boundary Lubricated Sliding. Tribol Lett. **17**, 553–559 (2004). https://doi.org/10.1023/B:TRIL.0000044504.76164.4e
33. Ranuša, M., Odehnal, L., Kučera, O., Nečas, D., Hartl, M., Křupka, I., et al.: Effect of Surface Texturing on Friction and Lubrication of Ti6Al4V Biomaterials for Joint Implants. Tribol Lett. **73**, 15 (2025). https://doi.org/10.1007/s11249-024-01950-5
34. Galandáková, A., Ulrichová, J., Langová, K., Hanáková, A., Vrbka, M., Hartl, M., et al.: Characteristics of synovial fluid required for optimization of lubrication fluid for biotribological experiments. J. Biomed. Mater. Res. B Appl. Biomater. **105**, 1422–1431 (2017). https://doi.org/10.1002/jbm.b.33663
35. Myant, C.W., Cann, P.: The effect of transient conditions on synovial fluid protein aggregation lubrication. J. Mech. Behav. Biomed. Mater. **34**, 349–357 (2014). https://doi.org/10.1016/j.jmbbm.2014.02.005
36. Myant, C., Underwood, R., Fan, J., Cann, P.M.: Lubrication of metal-on-metal hip joints: The effect of protein content and load on film formation and wear. J. Mech. Behav. Biomed. Mater. **6**, 30–40 (2012). https://doi.org/10.1016/j.jmbbm.2011.09.008
37. Nečas, D., Vrbka, M., Marian, M., Rothammer, B., Tremmel, S., Wartzack, S., et al.: Towards the understanding of lubrication mechanisms in total knee replacements – Part I: Experimental investigations. Tribol Int. **156**, 106874 (2021). https://doi.org/10.1016/j.triboint.2021.106874
38. Nečas, D., Vrbka, M., Galandáková, A., Křupka, I., Hartl, M.: On the observation of lubrication mechanisms within hip joint replacements. Part I: Hard-on-soft bearing pairs. J. Mech. Behav. Biomed. Mater. **89**, 237–248 (2019). https://doi.org/10.1016/j.jmbbm.2018.09.022

39. Odehnal, L., Ranuša, M., Čípek, P., Malý, M., Mazánová, V., Dlouhý, A., et al.: Additively manufactured Ti6Al4V with controlled surface structure as a potential material for joint implants: Long-term wear performance and durability. Tribol Int. **216**, 111599 (2026). https://doi.org/10.1016/j.triboint.2025.111599
40. Anil, M., Ahmed, S.F., Yi, J.W., Moon, M.-W., Lee, K.-R., Kim, Y., et al.: Tribological performance of hydrophilic diamond-like carbon coatings on Ti–6Al–4V in biological environment. Diam. Relat. Mater. **19**, 300–304 (2010). https://doi.org/10.1016/j.diamond.2009.12.001
41. XU, T.: Diamond-like carbon coatings for orthopaedic applications: an evaluation of tribological performance. J. Mater. Sci. Mater. Med. **10**, 83–90 (1999). https://doi.org/10.1023/A:1008916903171
42. Ghosh, S., Choudhury, D., Roy, T., Bin Mamat, A., Masjuki, H.H., Pingguan-Murphy, B.: Tribological investigation of diamond-like carbon coated micro-dimpled surface under bovine serum and osteoarthritis oriented synovial fluid. Sci. Technol. Adv. Mater. **16**, 035002 (2015). https://doi.org/10.1088/1468-6996/16/3/035002
43. Nečas, D., Gelnar, A., Rothammer, B., Marian, M., Ranuša, M., Wartzack, S., et al.: Frictional Behaviour and Surface Topography Evolution of DLC-Coated Biomedical Alloys. Biosurf Biotribol 2025;11. https://doi.org/10.1049/bsb2.70004
44. Guo, F., Dong, G., Qin, L., Zhang, D., Guo, J.: Tribological performance of DLC coating under aqueous solutions. Lubr. Sci. **31**, 262–272 (2019). https://doi.org/10.1002/ls.1461
45. Wu, B., Zhang, T., Deng, Q., Leng, Y., Huang, N.: Effects of Adsorption of Albumin and Gamma-Globulin on the Tribological Performance of a Diamond-Like Carbon Film. J. Wuhan Univ. Technology-Mater Sci. Ed. **34**, 1103–1108 (2019). https://doi.org/10.1007/s11595-019-2166-z

Figures

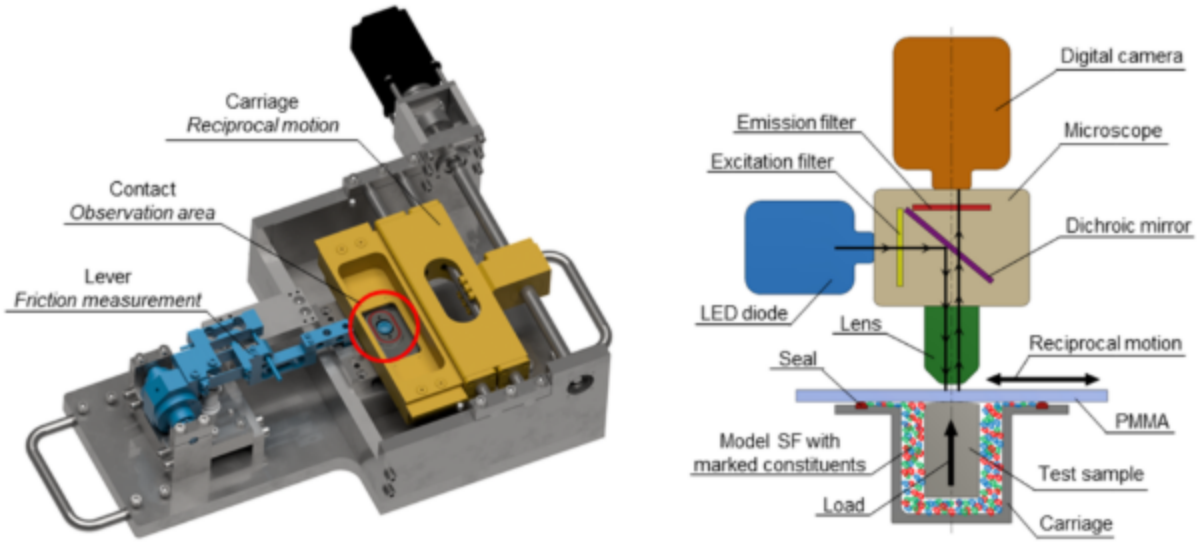

Figure 1

Schematic representation of the experimental apparatus: pin-on-plate tribometer (left) and fluorescence microscopy (right) (Reproduced from [39]).

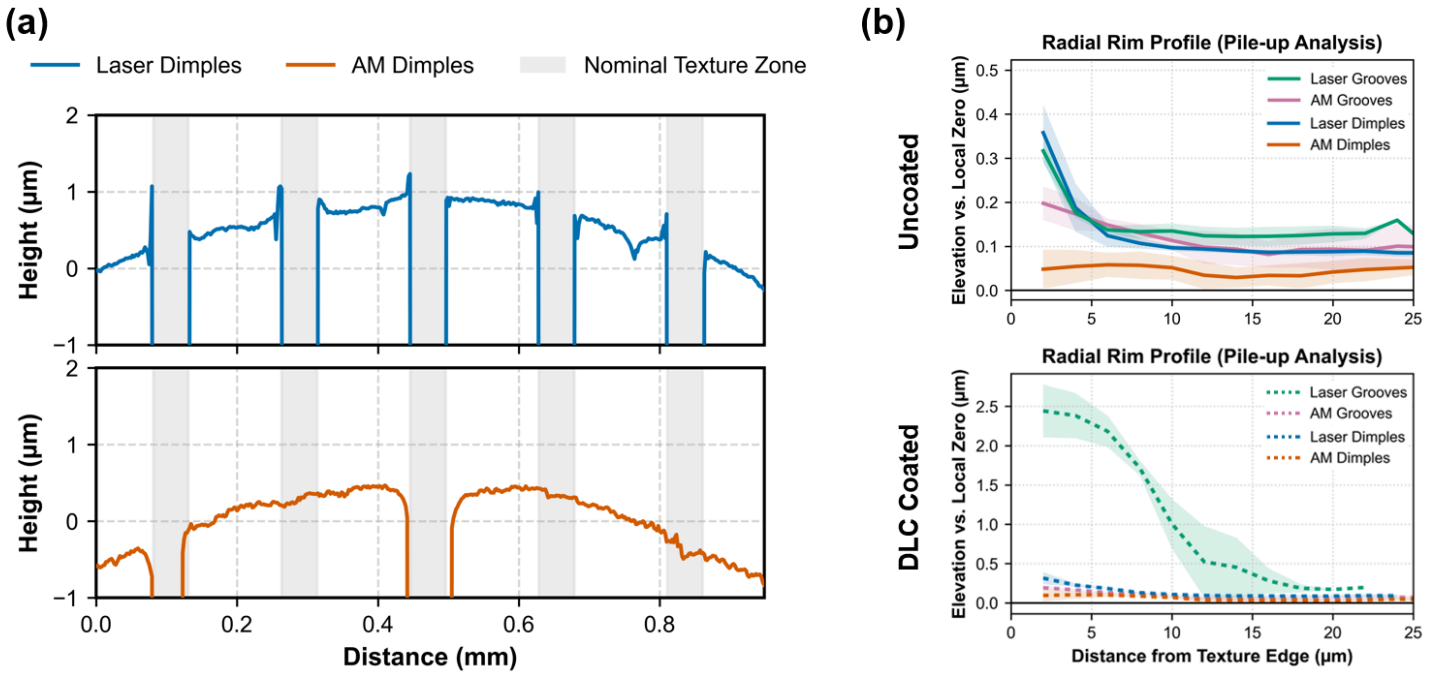

(c)	Laser dimples	Laser grooves	AM dimples	AM grooves
Area coverage (%)	5.82±0.32	16.98±0.57	1.55±0.33	19.24±9.42
Average diameter / width (µm)	49.02±4.13	36.82±8.25	25.72±14.68	45.00±41.05

Figure 2

(a) 2D cross-sectional profiles comparing edge morphology; (b) Mean radial profiles of the texture edges; (c) Area coverage and average dimension for each type of texture.

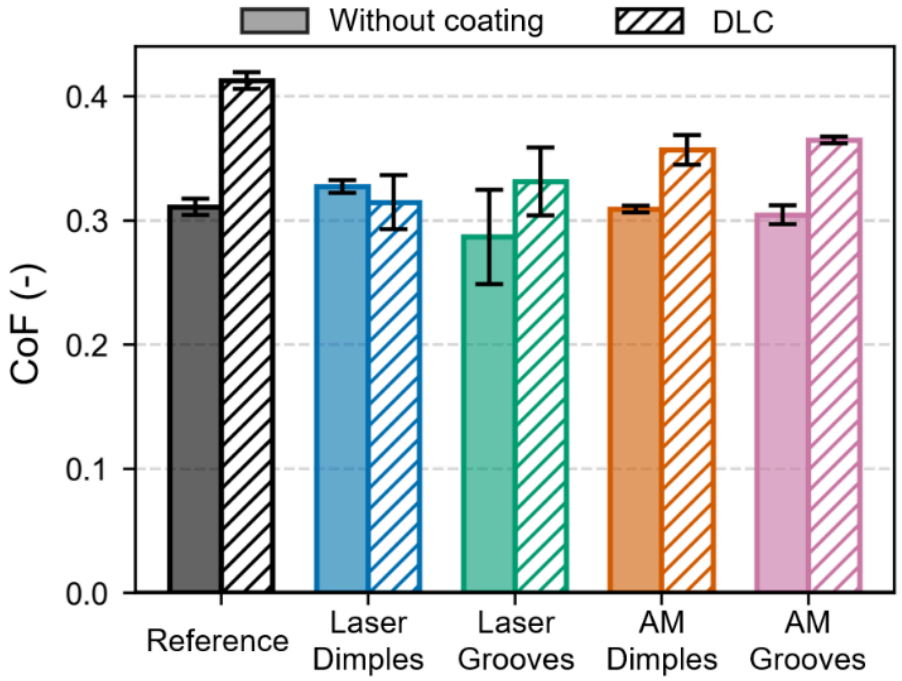

Figure 3

Mean values of CoF of the reference, laser-textured, and AM surfaces with and without a DLC coating at the stabilised post-run-in phase.

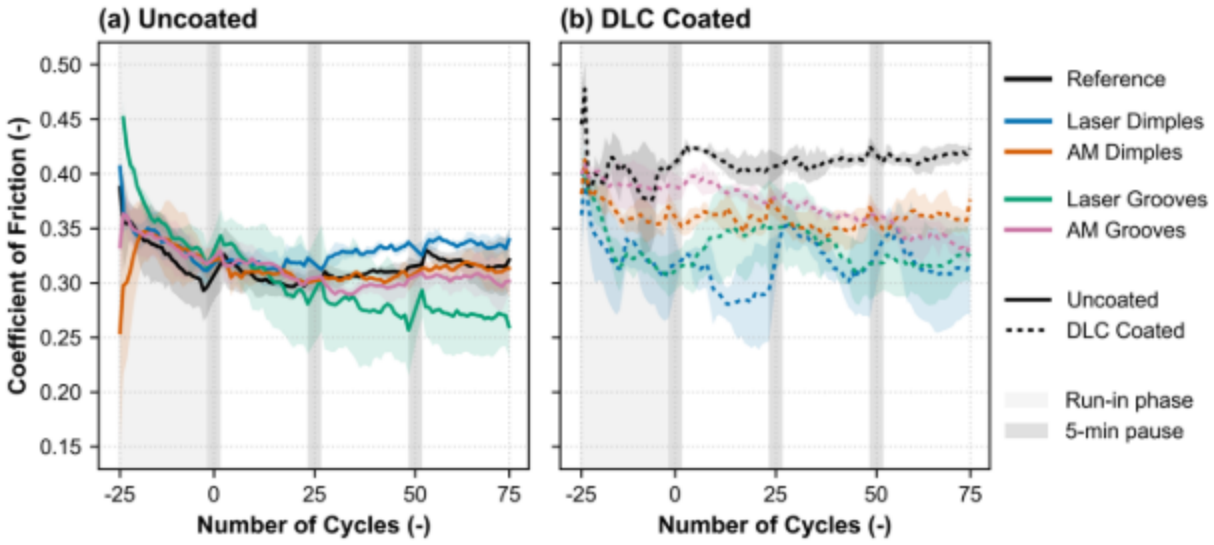

Figure 4

Time evolution of the macroscopic CoF for: (a) uncoated and (b) DLC-coated surfaces. (Solid and dotted curves represent the moving average, Coloured semi-transparent envelopes indicate the standard deviation.)

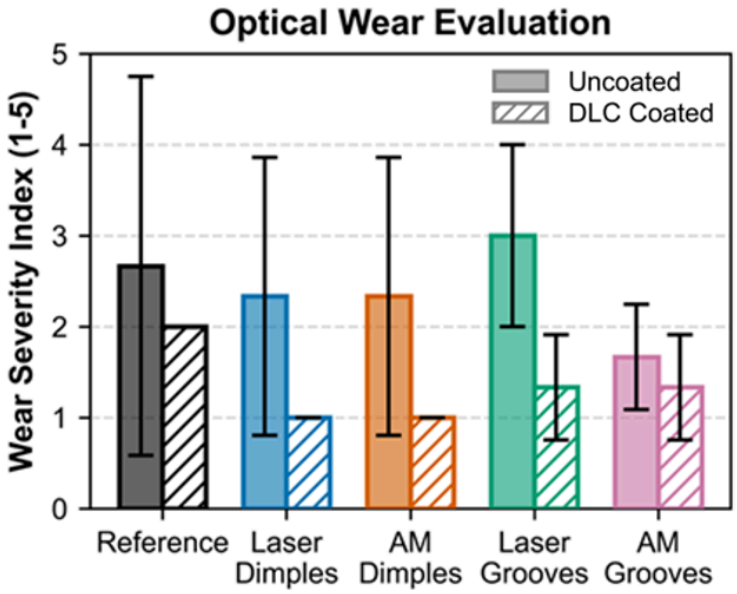

Figure 5

Semi-quantitative optical evaluation showing the optical wear severity index.

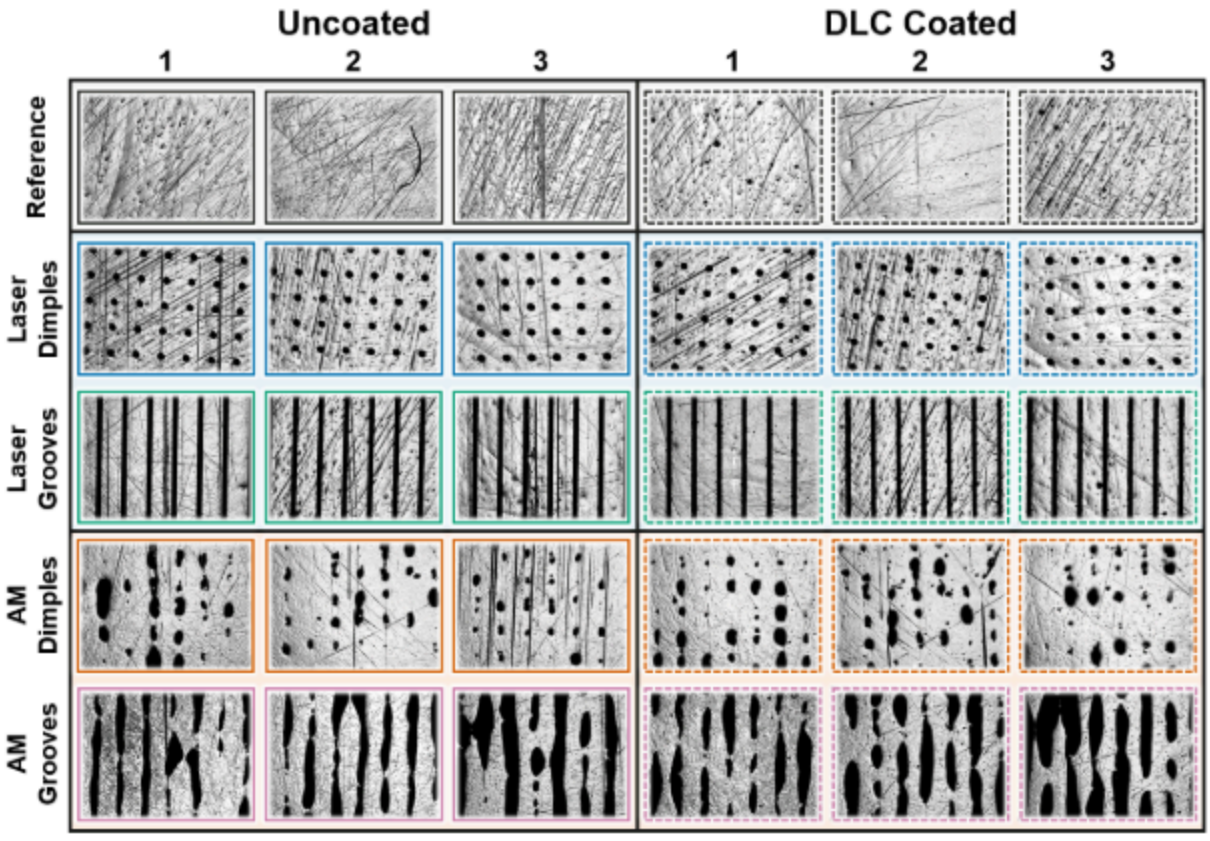

Figure 6

Representative optical images of the contact areas for all specimens.

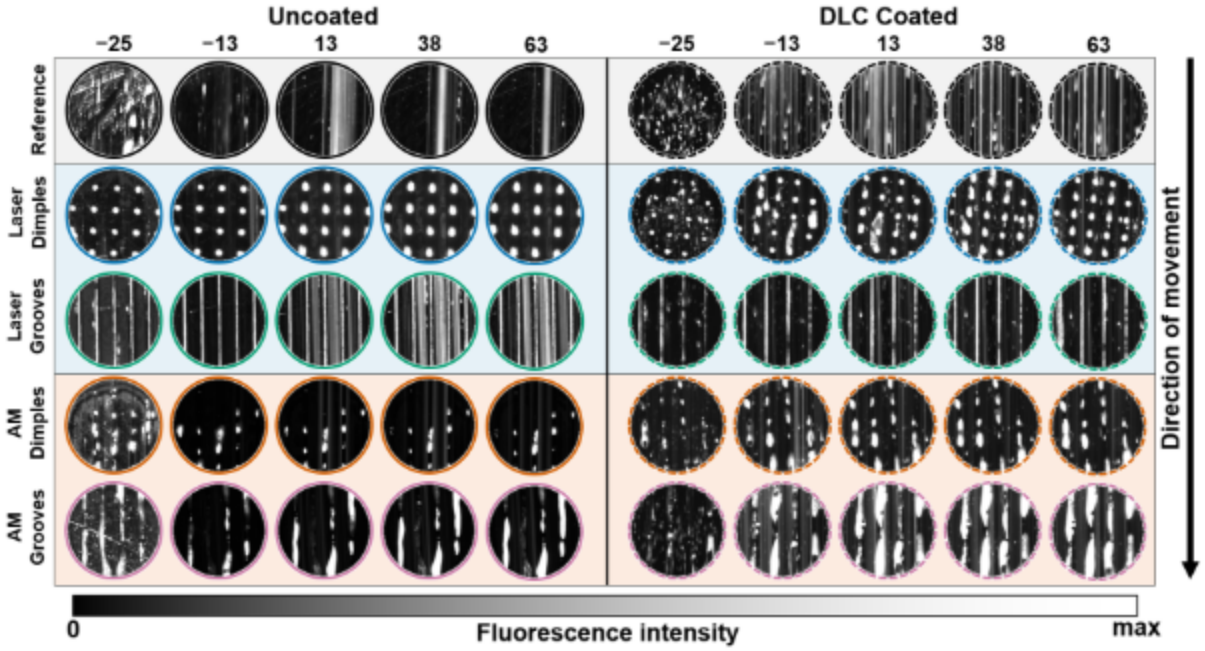

Figure 7

Time sequence of representative in-situ fluorescence microscopy images captured at cycles −25, −13, 13, 38, and 63.

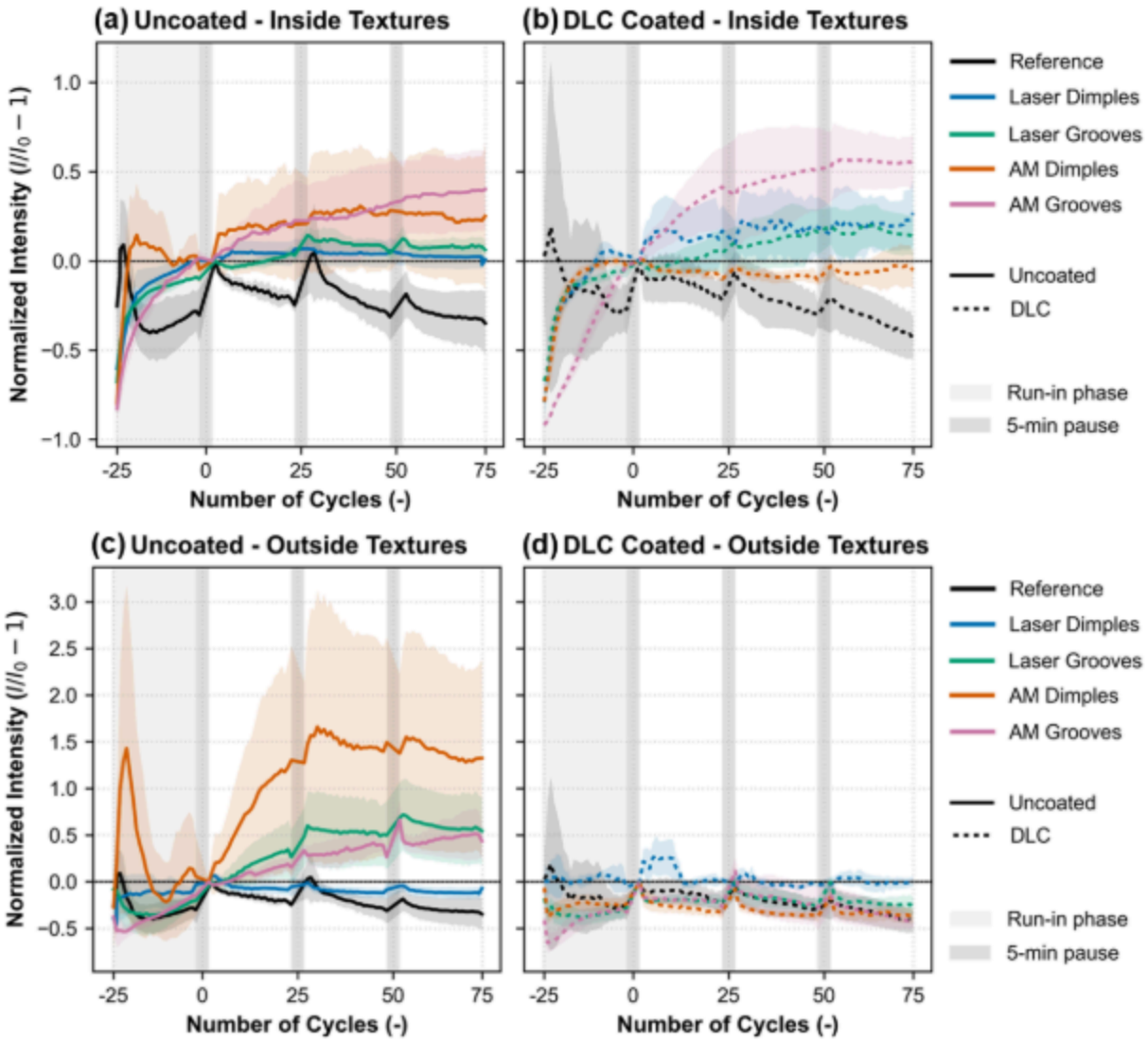

Figure 8

Time evolution of the normalised fluorescence intensity evaluated inside the textures: (a) uncoated and (b) DLC-coated surfaces, and outside the textures: (c) uncoated and (d) DLC-coated surfaces.

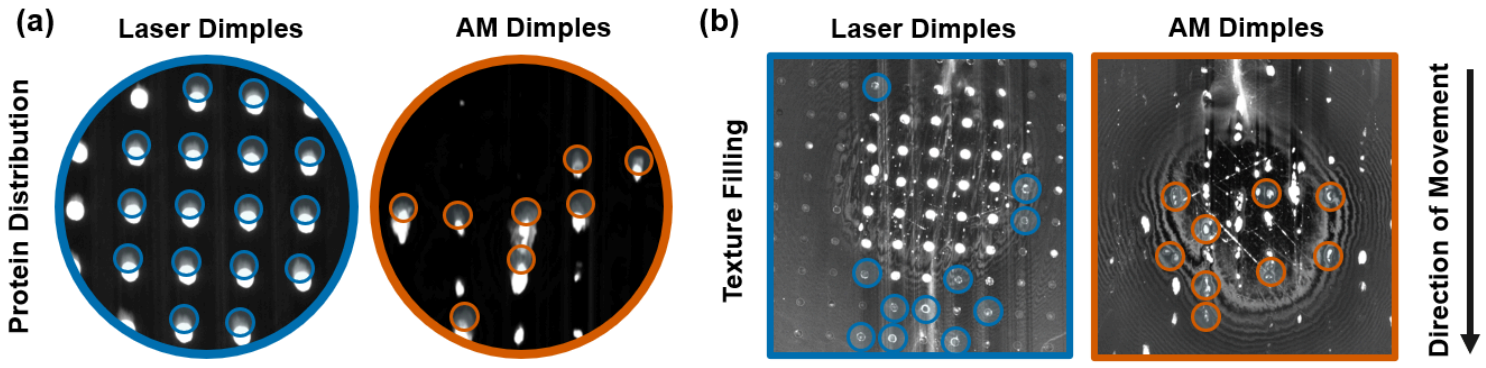

Figure 9

(a) Formation of fluorescent "distribution tails", and (b) comparison of apparent filling patterns for laser-machined and additively manufactured dimples.